JOURNAL OF MATERIALS SCIENCE 19 (1984) 1917–1929

Structure and mechanical properties of a $Fe_{90}Zr_{10}$ amorphous alloy

KOZO OSAMURA, SHOJIRO OCHIAI
Department of Metallurgy, Kyoto University, Sakyo-ku, 606 Kyoto, Japan

SHINJI TAKAYAMA
Central Laboratory, Hitachi Ltd., Kokubunji, 185 Tokyo, Japan

The structure of a $Fe_{90}Zr_{10}$ amorphous alloy was investigated by means of small angle X-ray scattering as well as large-angle diffraction measurements. For as-quenched specimens, SAXS was found to be relatively weak, but spread over a wide scattering angle. After quantitative analysis, it was concluded that a compositional fluctuation occurs on a fine scale of about 0.6 nm. When the specimen was heat treated below the crystallization temperature, the amorphous structure changed to a more stable dual structure consisting of pure iron and a structure similar to Fe_3Zr. By prolonged heat treatment, the iron-rich regions crystallized initially from the amorphous state. An apparent correspondence was found to exist between the changes in the amorphous structure and in the mechanical properties. The microscopic phase separation within the amorphous state resulted in an increase of ultimate tensile strength and fracture toughness. The deterioration of mechanical properties was suggested to be attributed to the gradual crystallization of iron-rich regions.

1. Introduction

Lack of periodicity on a macroscopic scale in amorphous alloys results in difficulty of structure analysis. At present, no general and objective methodology for the description and classification of amorphous structures has been fully established experimentally or theoretically. Methods used to study the structure experimentally include the derivation of the radial distribution function from diffraction experiments, the internal magnetic field from Mössbauer spectroscopy and the probability function from EXAFS experiments and so on. This information is available in short range scale among nearest and/or several neighbour atoms. Secondly, further information on a longer range scale may be obtained by high resolution transmission electron microscopy, atom-probe field ion microscopy and small angle scattering techniques and so on. These could be considered as information on an intermediate scale because the experiments give significant data in the range of several angstroms to 100 nm. The latter intermediate scale information will become important in considering the spatial homogeneity of amorphous structures.

A Fe–Zr amorphous alloy is one example of typical metal–metal amorphous alloy systems. The investigations, with respect to the amorphous structure, have so far been limited. The radial distribution function was obtained by several authors [1, 2]. Mössbauer studies have been made by Oshima *et al.* [3] and Hosoma and Nanao [4]. Ohnuma *et al.* [5] reported the stability of amorphous structures by magnetic measurements. Janick and Matyja [6] investigated the crystallization process in $Co_{90}Zr_{10}$ amorphous alloy.

In the present work, both small angle X-ray scattering (SAXS) and large angle diffraction measurements were performed to examine the structure of an amorphous alloy and its change during heat treatments. Also the mechanical properties were investigated in conjunction with the change of microstructure.

0022–2461/84 $03.00 + .12

2. Experimental methods

An amorphous $Fe_{90}Zr_{10}$ alloy was made by the ordinary single drum technique under a vacuum of 10^{-3} torr. Two types of amorphous ribbons with different cross-sections were prepared for the SAXS measurements (0.013 mm × 5 mm) and the mechanical test (0.026 mm × 2 mm). For the heat treatment, the specimen was placed in an evacuated glass tube and then annealed at various temperatures. From the preliminary DSC measurement, the crystallization temperature (T_x) was determined to be 763 K, when the specimen was heated at a rate of 5 K min^{-1}.

For absolute SAXS measurements, Mo$K\alpha$ radiation was generated by a Rigaku power supply operated at 50 kV and 160 mA. The incident beam was limited by using a Kratky type U-slit. As pointed out previously [7], the coherent scattered intensity, $J_{coh}(s)$, from amorphous alloys was very weak in comparison with other scattering sources such as fluorescence, $J_{fl}(s)$, and parastic scattering, $J_{BG}(s)$. The observed intensity, normalized by the intensity from the standard material, $E(s)/E_0$, was expressed as the equation [8],

$$E(s)/E_0 = tTJ_{coh}(s) + tTJ_{fl}(s) + TJ_{BG}(s) \quad (1)$$

where s is the scattering vector, t is the sample thickness and T is the transmission. After the subtraction of fluorescence and parastic terms, the corrected intensity was desmeared into the point-beam intensity, $I_{coh}(s)$ by using a computer program [8]. In order to check the structure change during the heat treatment, the diffraction intensity was measured over a wide range of scattering angle by a $2\theta - \theta$ diffractometer in transmission geometry. The tensile test was performed using an Instron-type testing machine with a strain rate of 1.3×10^{-3} sec^{-1} at room temperature. Vickers microhardness was measured under a load of 100 g. The fracture surface was observed with a scanning electron microscope (SEM).

3. Experimental results

3.1. Large-angle diffraction

Fig. 1 shows the result of diffraction measurements using Mo$K\alpha$ radiation at 45 kV and 80 mA. The first and second halo peaks were observed for specimens aged at temperatures below T_x. For the specimen aged at 823 K for 0.6 ksec, clear diffraction peaks due to an α-iron crystalline phase was observed, where the diffuse scattering remained still around the (1 1 0) peak. The lattice constant of the crystalline phase was determined to be 0.2860 ± 0.0002 nm, which is slightly smaller than the reported value of 0.2866 nm [9]. When the alloy was aged at 623 K for various periods, the half width of the first halo decreased by 3% on ageing for 60 ksec, and by 17% for 600 ksec. As shown in Fig. 1, the first halo for the specimen aged at 623 K for 600 ksec was sharpened and the peak position approached that of the diffraction peak of α-iron. When the alloy was annealed at various temperatures for 0.6 ksec, the half width decreased with increasing temperature. For instance, a 3% reduction for the specimen aged at 653 K and a 10% reduction at 773 K. From the above data, it is suggested that the first crystalline phase to appear from the amorphous state was α-iron and the crystallization progressed gradually during the heat treatment at temperatures below T_x.

3.2. Small angle X-ray scattering

Fig. 2 shows the angular dependence of coherent scattering intensity for Fe–Zr amorphous alloy as-quenched and aged specimens at 623 K. Observation of the SAXS intensity suggests the existence of electron density fluctuations in the material. The gradual change of SAXS intensity during isothermal ageing suggests a change of atomic configuration within the amorphous state. The as-quenched specimen showed weak and broad scattered intensity, having a maximum at about $s = 1.5$ nm^{-1}, and the intensity reached over the scattering vector of 10 nm^{-1}. After the 0.6 ksec ageing, the intensity was biased to a lower scattering vector region. The intensity increased again on prolonged ageing.

Here, the relation between SAXS intensity and the electron density fluctuation is briefly discussed. When $\Delta\rho(r)$ is a deviation of electron density at a position r from the average density, the electron density–density correlation is defined by the equation,

$$\gamma(r) = \int \Delta\rho(r_1)\Delta\rho(r_1 + r)\,dr_1 \quad (2)$$

The electron density fluctuation may arise from two origins, that is, the disorder of number density and the compositional fluctuation. In the present case, the major part of the electron density fluc-

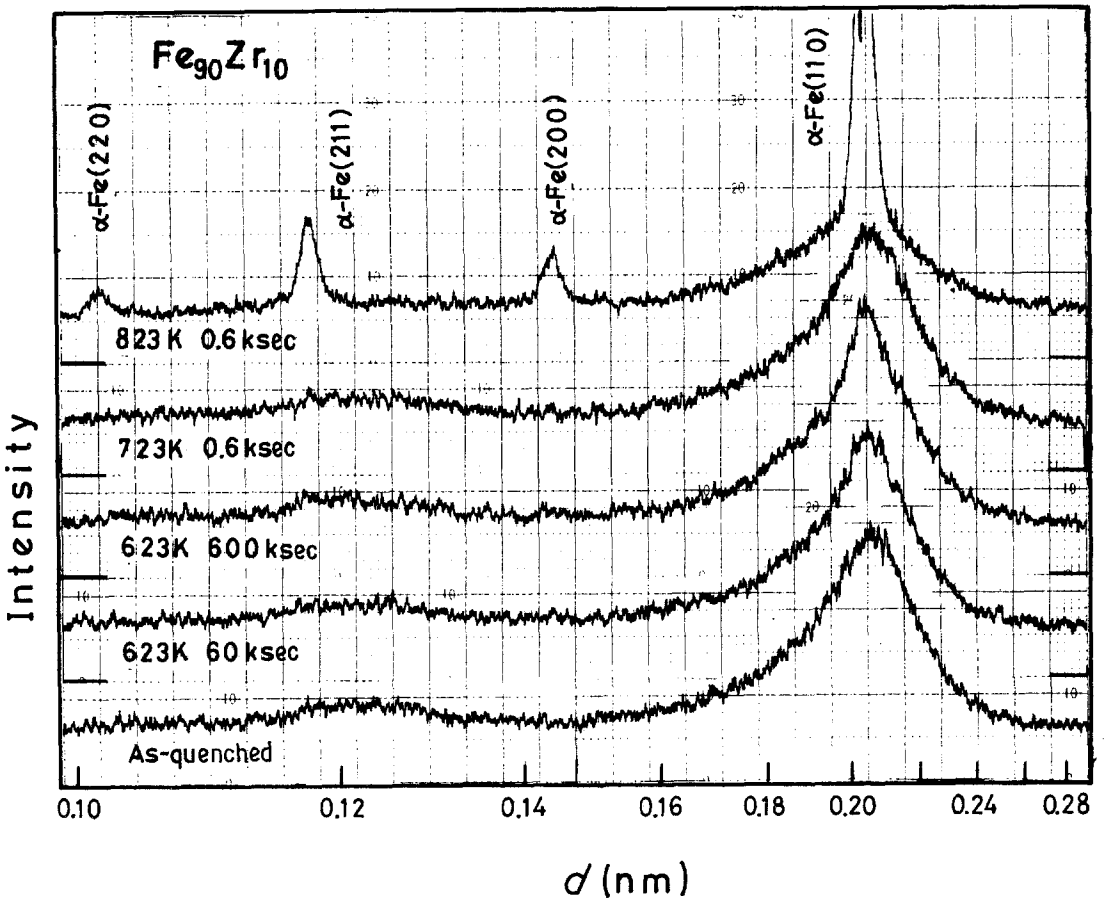

Figure 1 Large-angle diffraction patterns for the as-quenched and aged specimens of $Fe_{90}Zr_{10}$ amorphous alloy, where the ageing temperature and time are indicated in the figure.

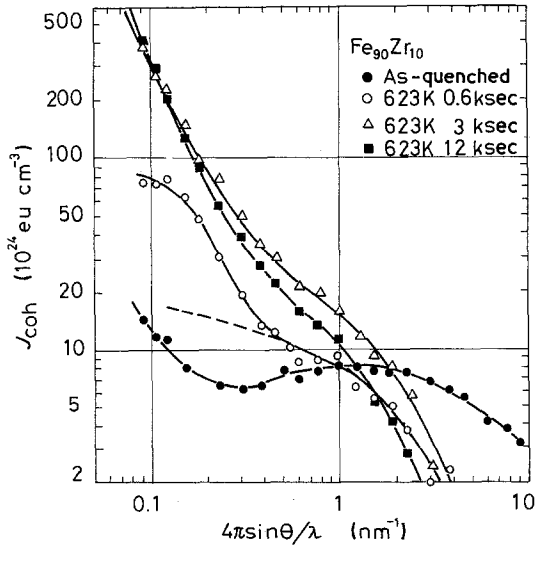

Figure 2 Angular dependence of absolute SAXS intensity for $Fe_{90}Zr_{10}$ amorphous alloy aged at 623 K.

tuation was thought to originate from the compositional fluctuation. As the SAXS intensity is related to the correlation by the equation,

$$I_{coh}(s) = I_0 \int_0^\infty 4\pi r^2 \gamma(r) \frac{\sin(sr)}{sr} dr \quad (3)$$

we can calculate directly the correlation function from the observed intensity, by Fourier inversion. The integrated intensity, defined by the following equation, depends upon square mean electron density fluctuation and the volume fraction,

$$\gamma(0) = (8\pi^3)^{-1} \int_0^\infty 4\pi s^2 I_{coh}(s)\, ds$$

$$= \langle \Delta\rho^2 \rangle V_f(1 - V_f). \quad (4)$$

Fig. 3 shows the normalized correlation as a function of radial distance. The correlation decreased rapidly for the as-quenched specimen and went down to zero at about 0.6 nm. This means that

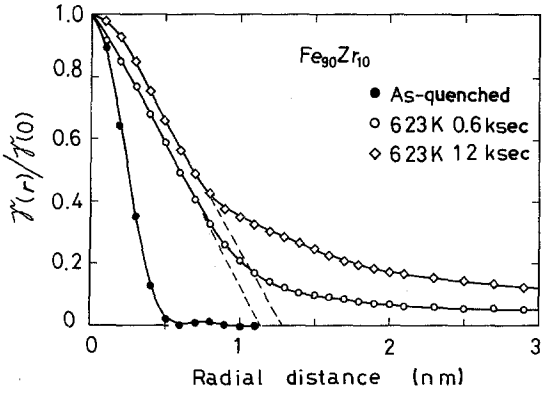

Figure 3 Normalized electron density–density correlation as a function of radial distance.

the compositional fluctuation occurred on a very fine scale. For the aged specimens, the correlation seemed to be divided into two parts. The first part is the strong correlation around the origin. The radial distance corresponding to zero correlation was determined by extrapolating the slope from the origin. This distance indicates the average size of fluctuated regions. The second characteristic feature is the rather weak and long-range correlation. With respect to the Fourier inversion given by Equation 3, the scattering intensity at the lower scattering vector region affects markedly the correlation at longer radial distances. For instance, the scattering intensity curve for the specimen aged at 623 K for 0.6 ksec shown in Fig. 2 might be divided into two parts by a dotted curve. It could be qualitatively said that the portion of the scattering intensity above the dotted curve is associated with the long-range correlation appearing in Fig. 3. This weak and long-range correlation increased during isothermal ageing accompanying with increasing the corresponding portion of the scattering intensity. The origin was discussed previously as arising from the interparticle interference [10].

The structural parameters analysed here are summarized in Table I. The integrated intensity was large for the as-quenched specimen, but decreased after the heat treatments. On the other hand, the size of fluctuated regions increased remarkably. These results suggest that a structural change occurred during the heat treatment. Hereafter, the structures of the as-quenched and of the aged specimens will be discussed separately.

The size of fluctuated regions was found to be 0.6 nm for the as-quenched specimen, which was too small to ensure those regions as a well-defined

TABLE I Observed integrated intensity and average size of compositionally fluctuated regions in $Fe_{90}Zr_{10}$ amorphous alloy

Condition of heat treatment	$\gamma(0)$ (10^{46} eu cm^{-6})	D (nm)
As-quenched	3.9	0.6
523 K 0.6 ksec	3.6	0.6
573 K 0.6 ksec	0.35	0.9
623 K 0.6 ksec	0.42	1.2
623 K 6 ksec	0.94	1.3
623 K 12 ksec	0.91	1.3
673 K 0.6 ksec	0.80	1.1
723 K 0.6 ksec	0.80	1.2

independent second phase. It is suggested that it is a compositional fluctuation in a so-called "amorphous solid solution". It is a mixture of constituent atoms with no long range periodicity for their configuration, but presumably having a local order between near neighbours. Here the average atomic volume was assumed to be expressed by the equation,

$$\bar{v} = 0.9v_{Fe} + 0.1v_{Zr} \quad (5)$$

where v_{Fe} and v_{Zr} are the partial atomic volumes of iron and zirconium atoms, respectively. The solid solution was assumed to be separated into two regions with respect to solute concentration. One includes solute atoms, but the other consists of pure iron atoms. Then the electron density of each region is given by the equation,

$$\text{Region 1; } Fe_{1-y}Zr_y, \rho_1 = [(1-y)Z_{Fe} + yZ_{Zr}]/\bar{v} \quad (6a)$$

$$\text{Region 2; Fe, } \rho_2 = Z_{Fe}/\bar{v} \quad (6b)$$

where Z_i is the atomic number of i element. Two structural parameters, the volume fraction of region 1 and the integrated intensity, were derived as follows,

$$V_{f,1} = 0.1/y \quad (7a)$$

$$\gamma(0) = (\rho_1 - \rho_2)^2 V_{f,1}(1 - V_{f,1}) \quad (7b)$$

The above two parameters were expressed as a function of y. When the observed integrated intensity listed in Table I was put in Equation 7b, the variables y and then the volume fraction $V_{f,1}$ could be determined. The result was that the solute concentration y in region 1 is about 0.4 and $V_{f,1}$ is about 0.25, respectively. Consequently, it is suggested that the size of fluctuated regions listed in Table I is the dimension of region 1.

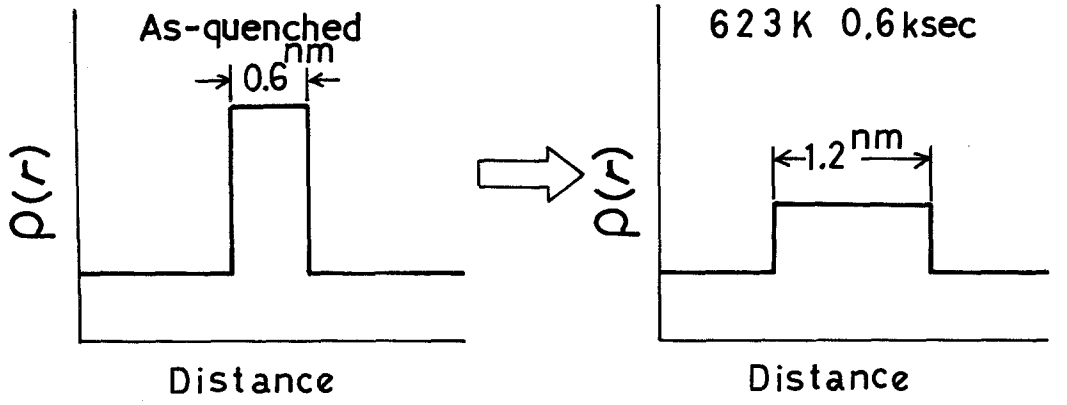

Figure 4 Schematic representation of the structure change by the heat treatment in $Fe_{90}Zr_{10}$ amorphous alloy.

When the alloy was heat treated, the integrated intensity decreased, but the size increased as shown schematically in Fig. 4. In order to explain this change, it was supposed that the structure of fluctuated regions changes to a more stable one. As listed in Table II, the structure was tentatively assigned to be similar to the structure of intermediate compounds. Then various sets of dual structure of pure iron and those compounds were examined. Comparing with the experimental data, the most probable phase was Fe_3Zr. However, it is not necessary for the actual fluctuated regions to correspond to a rigid compound, but it is suggested that they have a similar electron density at least.

Fig. 5 shows the angular dependence of SAXS intensity for the specimens aged at various temperatures for 0.6 ksec. The intensity for the specimen aged at 523 K was similar to that of the as-quenched one in the higher scattering vector region, but was larger in the lower region. The existence of scattered intensity beyond the scattering vector of 10 nm^{-1} suggests that the structure is essentially the same as that of the as-quenched specimen. However, the long range correlation of compositional fluctuation increased because the intensity at the lower scattering region became larger. The angular dependence of scattered intensity for the specimens aged above 623 K was different from that for the as-quenched specimen. Especially in the higher scattering vector region, the intensity decreased remarkably. This is attributed to an increasing size of fluctuated regions, as discussed in the above paragraph. Its step of structure change might be called "microscopic phase separation" within the amorphous state, since the major part of the large-angle diffraction was the halo pattern in the heat-treatment conditions with the shorter ageing times less than 10 ksec at 623 K and the lower temperatures less than 650 K for 0.6 ksec. As seen in Table I, the solute enriched regions tended to increase slightly in size and in total amount with increasing isochronal ageing temperature and isothermal ageing time. On the other hand, region 2, whose composition was assumed to be pure iron, was suggested to crystallize preferentially during the prolonged heat treatment as implied by the result mentioned in Section 3.1.

TABLE II Structural parameters for some compounds appearing in Fe–Zr binary alloy system, where ρ is the electron density per unit volume, $\gamma(0)$ is the integrated intensity and $V_{f,comp.}$ is the volume fraction occupied by the compound. Both $\gamma(0)$ and $V_{f,comp.}$ were calculated assuming that the $Fe_{90}Zr_{10}$ alloy decomposed into the pure iron and the respective compound

Compound	Crystal structure	ρ (10^{24} eu cm^{-3})	$\gamma(0)$ (10^{46} eu cm^{-6})	$V_{f,comp.}$
$Fe_{23}Zr_6$	$D8_4$ [15] a = 1.2 nm	1.940	1.78	0.54
Fe_3Zr	$E9_3$ [15] a = 1.169 nm	2.068	0.48	0.45
Fe_2Zr	$C15$ [16] a = 0.705 nm	2.100	0.26	0.35

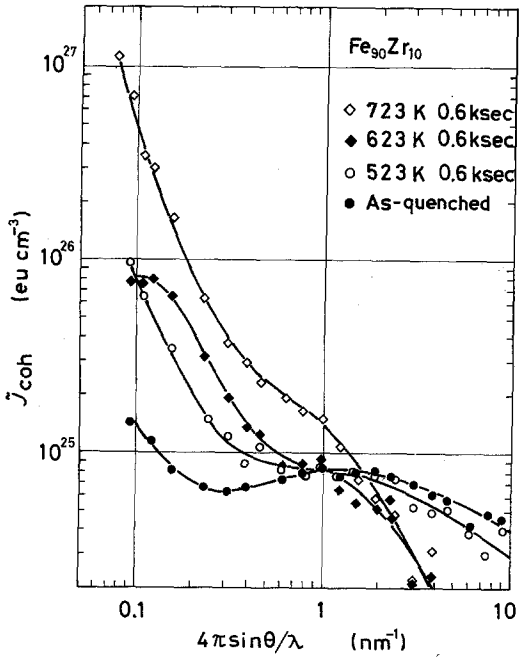

Figure 5 Angular dependence of absolute SAXS intensity for $Fe_{90}Zr_{10}$ amorphous alloy aged at various temperatures for 0.6 ksec.

3.3. Mechanical test

Fig. 6 shows the time evolution of Vickers microhardness for the specimens aged at 623 K. The value increased moderately up to about 10 ksec ageing, beyond which the hardness increased. Fig. 7 shows the change of ultimate tensile strength (UTS), where the average value was obtained for 5 to 10 specimens and the maximum was the highest measured value. Comparing with the change of hardness, the average strength remained nearly constant during ageing up to 10 ksec, after which the strength decreased with increasing ageing time. The ageing behaviour of both mechanical properties could be apparently divided into two stages by taking a specific ageing time, that is, 10 ksec. The ratio, H_v/σ_{UTS} has been examined as a function of ageing time as shown in Fig. 8. The ratio, H_v/σ_Y was reported [11] to be about 3.2, when the amorphous alloy shows yielding. In the present Fe–Zr alloy, the exact value of yield stress σ_Y could not be determined because of the small fracture strain. Therefore σ_{UTS} was used instead of σ_Y in the present discussion. As shown in Fig. 8, the ratio became 3.6 for the as-quenched specimen, which was slightly larger than the reported value. In the early stage of ageing, the ratio remained mostly constant, but increased remarkably beyond the isothermal ageing time of 10 ksec.

Fig. 9 shows the change of hardness during the isochronal ageing, where each specimen was held for 0.6 ksec at each temperature. The behaviour seemed to be similar to the case of isothermal ageing as shown in Fig. 6. The hardness increased slightly with increasing temperature up to 650 K. Owing to the partial crystallization, the hardness increased at higher temperatures, as discussed later. The corresponding change of tensile strength is shown in Fig. 10. The average value increased appreciably after the ageing at 423 K compared with the as-quenched value. When the specimen was aged above the crystallization temperature, the strength decreased substantially. The ratio H_V/σ_{UTS} as a function of isochronal ageing

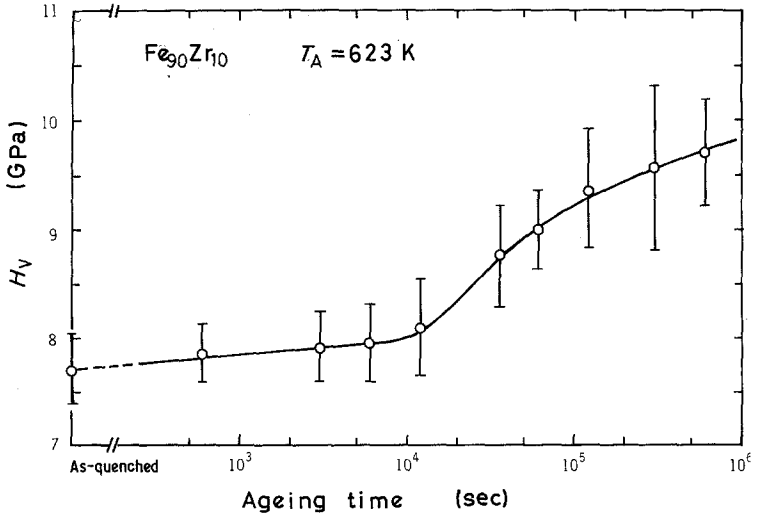

Figure 6 Ageing-time dependence of Vickers microhardness for $Fe_{90}Zr_{10}$ amorphous alloy aged at 623 K.

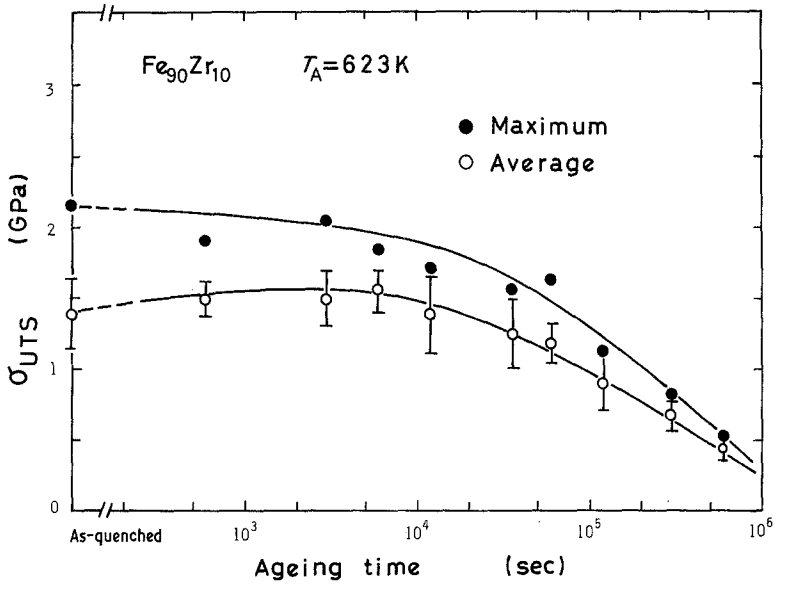

Figure 7 Ageing-time dependence of ultimate tensile strength for $Fe_{90}Zr_{10}$ amorphous alloy aged 623 K, where ○ and ● show the average and the maximum values, respectively, and the error bar is the standard deviation.

temperature is shown in Fig. 11, where the marked increase seemed to have started at around 650 K. The apparent stress intensity factor of type I, K_Q, was measured by using the foil specimen with one side notch and the results are shown in Fig. 12. In the lower temperature range, K_Q showed a higher value than that of the as-quenched specimen. When the alloy was aged at higher temperatures, K_Q decreased continuously beyond the crystallization temperature.

3.4. Scanning electron microscopic observation

As shown in Figs. 7, 8, 10 and 11, the change of tensile strength σ_{UTS} and brittleness H_V/σ_{UTS} showed two stages as a function of ageing temperature or time. In the first stage, where the specimens were isochronally aged for 0.6 ksec below 650 K or isothermally aged at 623 K for the period below 10 ksec, they showed high σ_{UTS} and high ductility, but in the second stage,

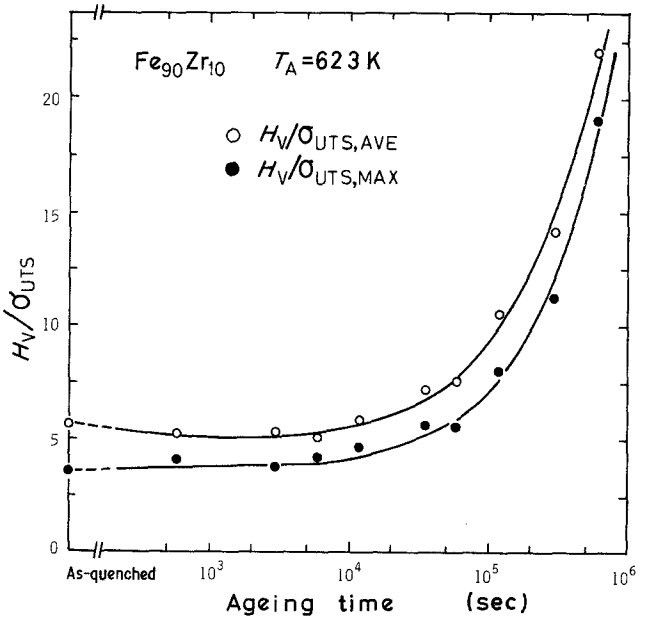

Figure 8 Change of the ratio, H_V/σ_{UTS} as a function of ageing time.

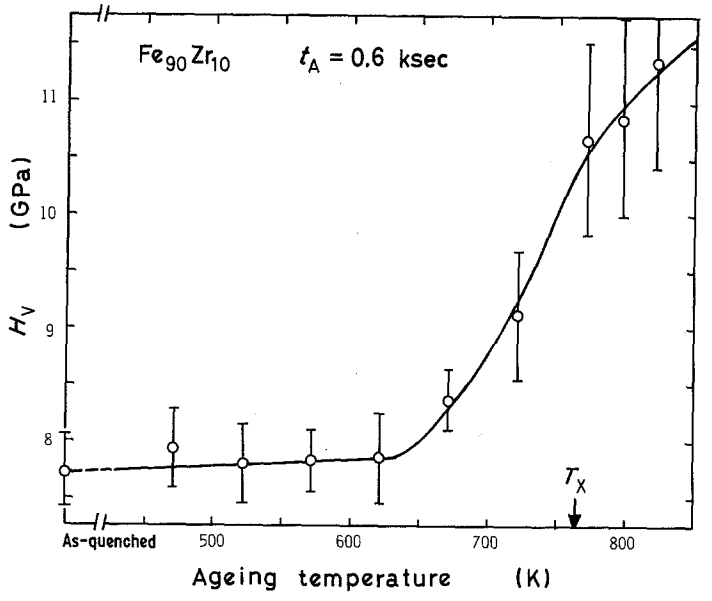

Figure 9 Temperature dependence of Vickers microhardness for $Fe_{90}Zr_{10}$ amorphous alloy aged at various temperatures for 0.6 ksec.

where they were isochronally aged at higher temperatures or isothermally aged for longer periods, they showed low σ_{UTS} and low ductility. The feature of the fracture surface of each stage can be summarized as follows.

In the first stage, four patterns were in general observed; a fibrous zone (FZ) as in Fig. 13a, a vein pattern (VP) and a featureless zone (FLZ) as in Figs. 13b and c, and a shallow dimpled pattern (SDP) as in Fig. 13c. In most specimens, the fracture started from the free surface, accompanying the FZ. Following the FZ, VP, FLZ and SDP appeared. The area occupied by the SDP for the specimens with high σ_{UTS} was narrow, but that of specimens with low σ_{UTS} was wide. However, for the specimen aged at 523 K for 0.6 ksec, which had the highest σ_{UTS}, the starting point of fracture existed inside the specimen and the fracture surface was wholly covered by both VP and FLZ except a small region of SDP as shown in Fig. 13d. The fracture surface of VP and FLZ was inclined 45–50° to the tensile axis but that of the SDP was perpendicular to the tensile axis, as shown in Fig. 13e. When σ_{UTS} was low, a chevron pattern was superposed on SDP as in Fig. 13f.

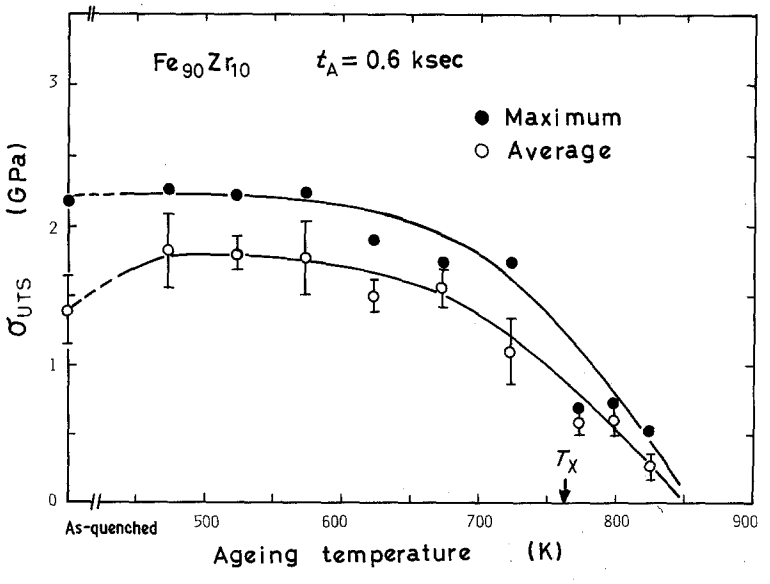

Figure 10 Temperature dependence of ultimate tensile strength for $Fe_{90}Zr_{10}$ amorphous alloy aged at various temperatures for 0.6 ksec.

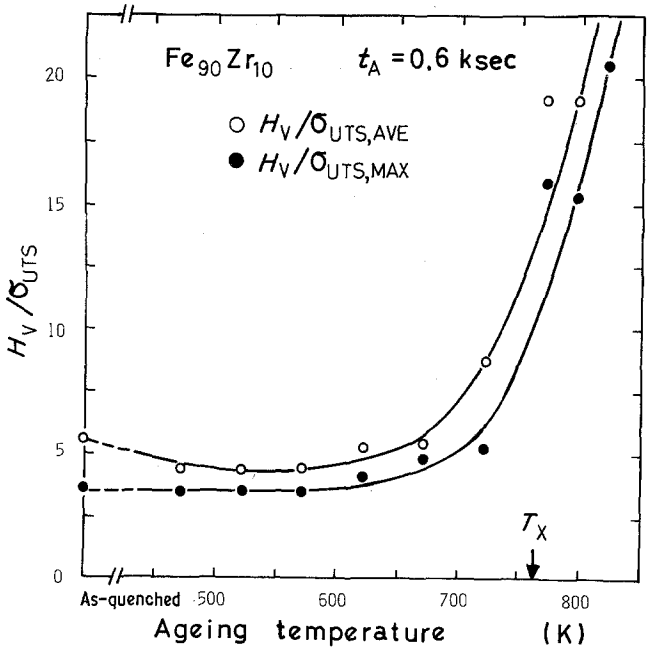

Figure 11 Change of the ratio, H_v/σ_{UTS} as a function of ageing temperature.

In the second stage, the area occupied by VP and FLZ decreased and that occupied by SDP increased in comparison with those in the first stage. When σ_{UTS} was low, the SDP became very fine as shown in Figs. 14a and b, where the average interval of fine dimples was about 0.13 μm. When specimens had the same σ_{UTS}, the morphologies of the fracture surface were similar to each other, even if the ageing treatment was different, as shown in Figs. 14a and b; both specimens shown in (a) and (b) had the same value of σ_{UTS} = 0.57 GPa. When the ageing temperature exceeded 773 K in isochronal ageing, specimens showed a complete brittle fracture surface, with a hackle pattern, as shown in (c).

4. Discussion

In order to explain the origin of the SAXS intensity observed for the as-quenched specimen, a structure model was proposed, which assumed implicitly a distinct interface between two fluctuated regions. The result was that the amorphous structure could be described as an amorphous solid solution with two compositionally fluctuated

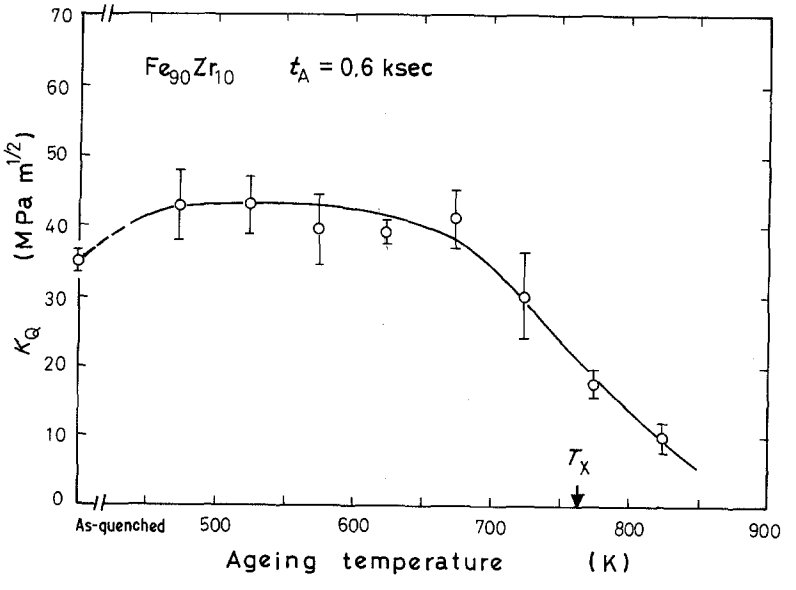

Figure 12 Change of the apparent stress intensity factor as a function of ageing temperature.

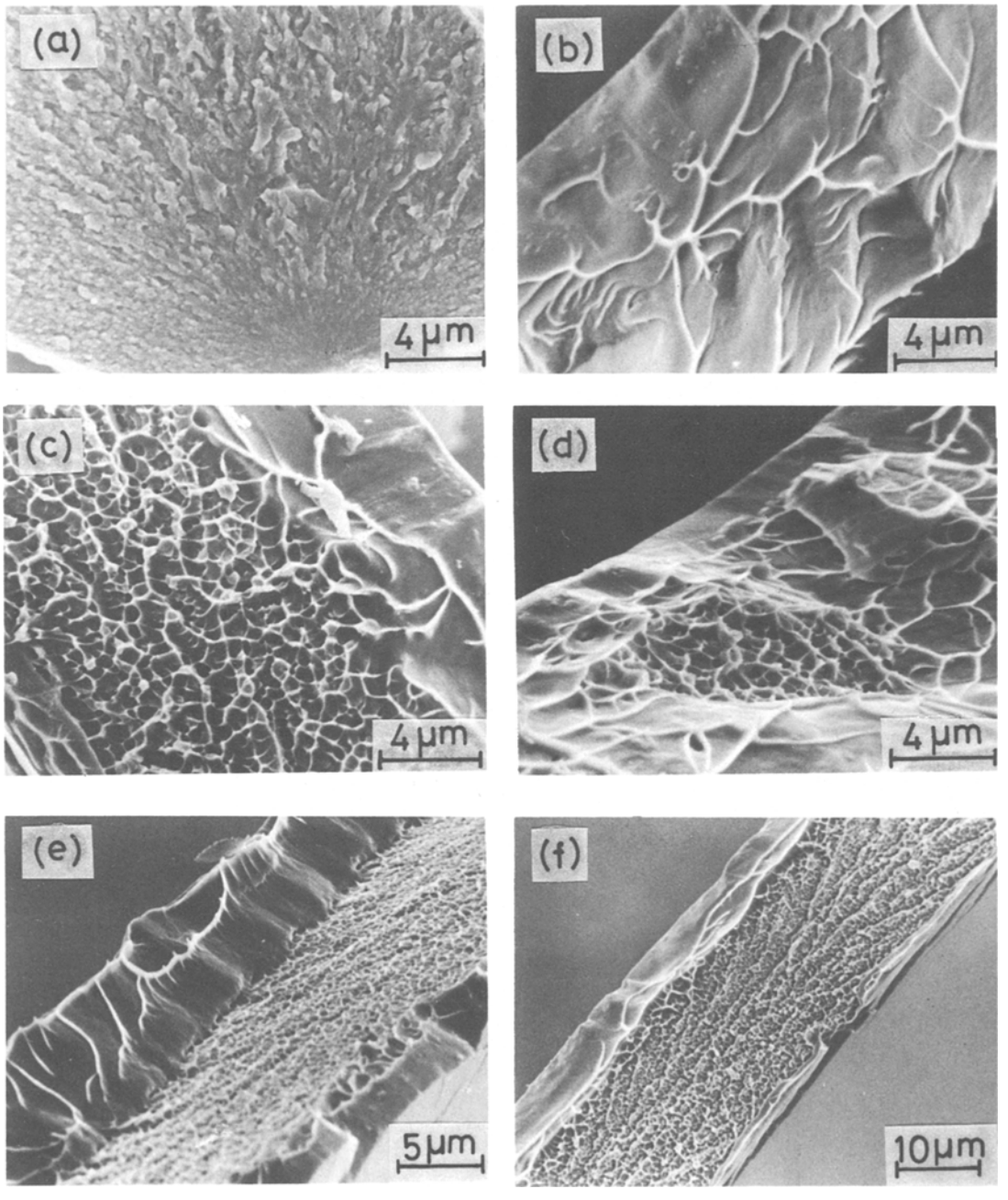

Figure 13 Fracture surfaces of the as-quenched and aged specimens in the first stage of heat treatment, where (a), (b), (c) and (f) are of the as-quenched specimens, and (d) and (e) are of the aged specimens at 523 K for 0.6 ksec, respectively.

regions represented by pure iron regions and zirconium-enriched regions. Although it is necessary to assume a distinct interface to simplify the analysis, it is unlikely that this would be the case in practice. If a diffuse interface was assumed, the resulting conclusion would not differ essentially from the present result. Recently, Oshima *et al.* [3] determined the distribution of internal magnetic field for the as-quenched $Fe_{90}Zr_{10}$ amorphous alloy by Mössbauer measurements. Two broad peaks, centred at 250 and 100 kOe, were present and their areal fraction was 0.8/0.2. They suggested that iron atoms are situated in two different magnetic environments. The above value of areal fraction, corresponding to the weaker magnetic field, is nearly consistent

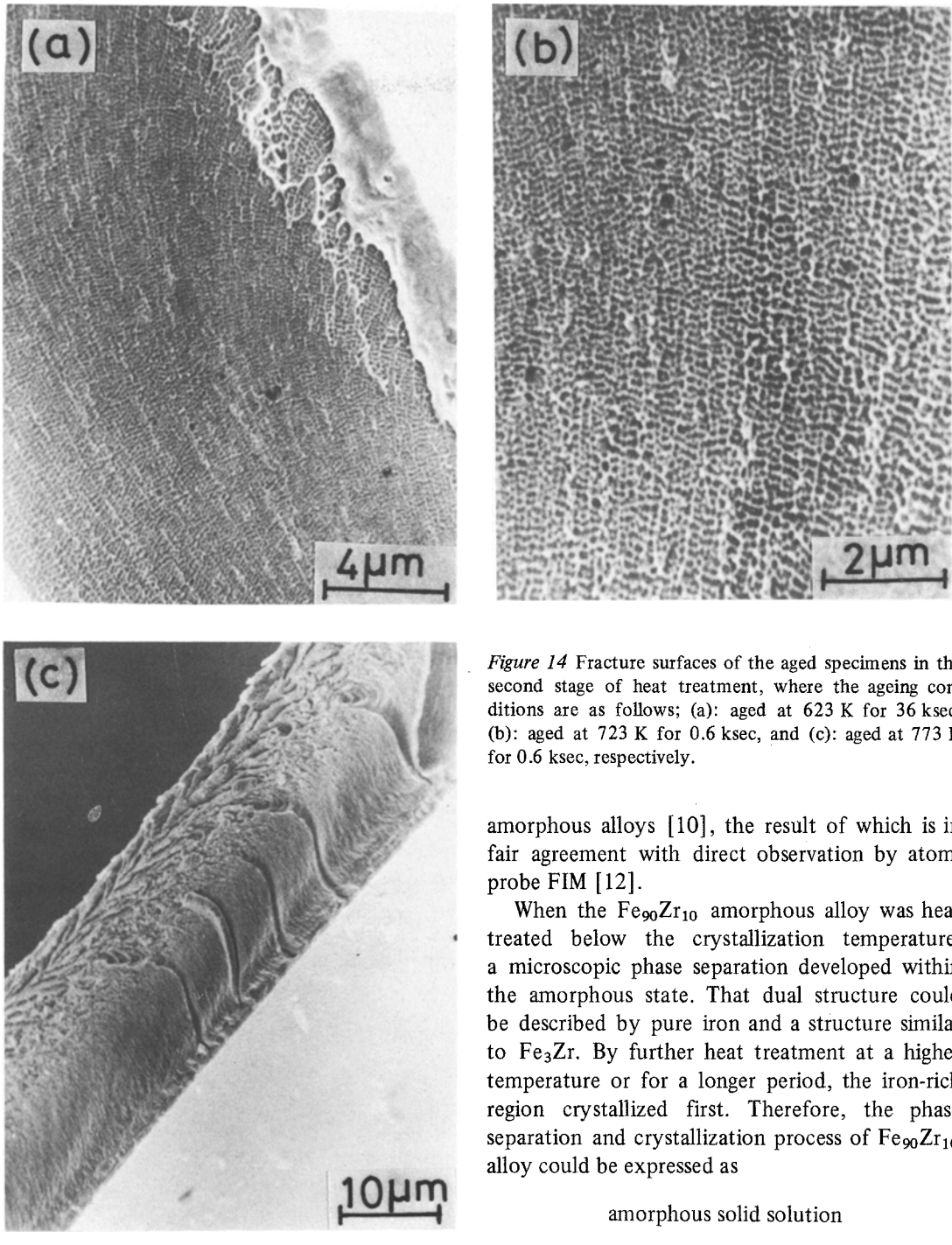

Figure 14 Fracture surfaces of the aged specimens in the second stage of heat treatment, where the ageing conditions are as follows; (a): aged at 623 K for 36 ksec, (b): aged at 723 K for 0.6 ksec, and (c): aged at 773 K for 0.6 ksec, respectively.

with the volume fraction of the region 1 determined by the present analysis. It might be noted that the present proposed structure is not an unique solution, but is one of the most probable structures derived from SAXS analysis. A similar analysis has been performed previously for Fe–B amorphous alloys [10], the result of which is in fair agreement with direct observation by atom-probe FIM [12].

When the $Fe_{90}Zr_{10}$ amorphous alloy was heat treated below the crystallization temperature, a microscopic phase separation developed within the amorphous state. That dual structure could be described by pure iron and a structure similar to Fe_3Zr. By further heat treatment at a higher temperature or for a longer period, the iron-rich region crystallized first. Therefore, the phase separation and crystallization process of $Fe_{90}Zr_{10}$ alloy could be expressed as

amorphous solid solution

$\longrightarrow$ phase separation (Fe/Fe_3Zr)

within the amorphous state

$\longrightarrow$ α-Fe + amorphous phase

$\longrightarrow$ α-Fe + Fe_3Zr

$\longrightarrow$ α-Fe + Fe_3Zr + Fe_2Zr

by combining the result reported by Oshima

TABLE III Summary of structure analysis for some metal–metalloid and metal–metal amorphous alloys by means of small angle X-ray scattering measurements

System	Alloy	As-quenched state		After ageing at T_A below T_x		
		D (nm)	Structure	T_A/T_x	D (nm)	Structure
Metal–Metalloid	$Fe_{83}B_{17}$ [10]	1.2	Similar to Fe/Fe_3B	0.82	Slightly decreased	Unchanged
	$Fe_{84}P_{10}C_6$ [7 17]	1.9	Similar to Fe/Fe_3 (P, C)	0.87	Slightly increased	Unchanged
Metal–Metal	$Fe_{90}Zr_{10}$	0.6	Amorphous solid solution	0.78	Increased	Similar to Fe/Fe_3Zr
	$Co_{90}Zr_{10}$ [13]	< 0.6	Amorphous solid solution	0.81	Increased	Similar to $Co/Co_{23}Zr_6$

et al. [3]. In a similar alloy system $Co_{90}Zr_{10}$, Janick and Matyja [6] reported that the crystallization process as amorphous $\longrightarrow$ β-Co + amorphous $\longrightarrow$ β-Co + $Co_{23}Zr_6$. The phase separation within the amorphous state has also been proposed as amorphous solid solution $\longrightarrow$ phase separation ($Co/Co_{23}Zr_6$) [13].

The characteristics of amorphous structures in several alloy systems are summarized as shown in Table III. From the viewpoint of long range compositional fluctuation in space, there is a difference of amorphous structure between metal–metal and metal–metalloid alloy systems. The amorphous structure of metal–metalloid glasses such as Fe–B system, is closely related to dual structure of iron and Fe_3B [10]. The particle-like scheme is appropriate for the analysis of structures. On heat treatment, their structure did not change in quality so much. On the other hand, the amorphous structure of metal–metal alloy systems was described as an amorphous solid solution, in which the atomic configuration is not homogeneous, but presumably a compositional fluctuation occurs with respect to the zirconium atoms. Even a short time ageing forces those fluctuations to change to a more stable state by undergoing phase separation within the amorphous state. The resulting dual structure is suggested to be analogous to the amorphous structure of metal–metalloid systems.

A phenomenological interrelation has been shown to exist between the microstructure and the mechanical properties. The temperature and ageing-time dependences of mechanical properties could be explained from the structure change characterized by X-ray analysis. In the early stage of ageing, the microscopic phase separation within the amorphous state resulted in an increase in ultimate tensile strength and fracture toughness. This might be attributed to the local atomic regrouping, according to which the microscopic stress concentration centres could be relaxed, and to the change towards a more stable atomic configuration, which could make the elastic moduli increase [14]. As shown in Fig. 12, higher values of stress intensity factor than that of the as-quenched specimen were realized on ageing at temperatures below 673 K. The highest value was observed for the specimen aged at 473 K for 0.6 ksec, at which complete phase separation had not occurred, although the transition was in progress.

The deterioration of mechanical properties was suggested to be attributed to the gradual crystallization of iron-rich regions. As shown in Figs. 8 and 11, a remarkable deterioration occurred at temperatures above 650 K for isochronal ageing and for the ageing periods above 10 ksec for isothermal ageing. Correspondingly, the decrease of the half width of the first halo was recognized and the diffraction peak due to α-Fe was observed on prolonged heat treatment. At this stage, it was suggested that the fine crystalline regions were dispersed homogeneously in the amorphous matrix. Under the applied load, due to the existence of these fine crystalline regions, the yield stress could increase as ageing proceeded, similar to that in normal age-hardenable alloys [18]. The change of the hardness, which had a strong relation to σ_Y, could be explained by this mechanism. On the other hand, the measured values of σ_{UTS} and K_Q decreased at higher temperatures for the isochronal ageing and for the longer ageing period for isothermal ageing. In these ageing stages, all specimens failed in a brittle manner in the simple tensile test, before they

showed distinct yield phenomenon in the stress–strain curve. This implies that, in these stages, stress concentration centers probably around fine crystalline regions led to premature fracture of specimens, resulting in loss in σ_{UTS}. Thus the ratio, H_v/σ_{UTS} shown in Figs. 8 and 11 is now understood to be a measure of brittleness; the higher the ratio, the lower the ductility.

5. Conclusion

In the present study, the sequence of phase separation and crystallization in a $Fe_{90}Zr_{10}$ amorphous alloy was made clear. Especially, the amorphous alloy was found to decompose into a more stable dual structure from an amorphous solid solution. On further heat treatment, the α-iron phase crystallized initially. Temperature and ageing-time dependences of mechanical properties could be satisfactorily interpreted in terms of these structure changes. The increase of ultimate tensile strength and fracture toughness was attributed to a microscopic phase separation within the amorphous state. The partial crystallization of iron-rich regions led to deterioration of the mechanical properties.

Acknowledgements

The authors express their hearty thanks to R. Suzuki and K. Shibue for their assistance. The present work was fulfilled partially by a Grant in Aid For Scientific Research (Project No. 56211030) of the Ministry of Education, Science and Culture of Japan.

References

1. N. C. HALDER and C. N. J. WAGNER, *J. Chem. Phys.* 47 (1967) 4385.
2. H. S. CHEN, K. T. AUST and Y. WASEDA, *J. Non-Cryst. Solid* 46 (1981) 307.
3. R. OSHIMA, M. TANIMOTO, F. E. FUJITA, N. NOSE and T. MASUMOTO, Proceedings of the 4th International Conference on Rapidly Quenched Metals (Japan Institute of Metals, Sendai, 1982) p. 1117.
4. T. HOSOMA and S. NANAO, *ibid.* p. 1125.
5. S. OHNUMA, Record of Autumn Meeting of Japanese Institute of Metals, (1980) 329.
6. A. J. JANICK and H. MATYJA, *J. Mater. Sci.* 15 (1980) 2317.
7. K. OSAMURA, K. SHIBUE, R. SUZUKI and Y. MURAKAMI, *Colloid Polym. Sci.* 259 (1981) 677.
8. K. OSAMURA and H. OKUDA, *J. Jpn. Inst. Met.* 47 (1983) 462.
9. "International Tables for X-Ray Crystallography", Vol. 3 (The Kynoch Press, 1968) p. 281.
10. K. OSAMURA, K. SHIBUE, R. SUZIKI, S. TAKAYAMA and Y. MURAKAMI, *J. Mater. Sci.* 16 (1981) 957.
11. L. A. DAVIS, "Metallic Glasses" (ASM, Ohio, 1978) p. 191.
12. J. PILLER and P. HAASEN, *Acta Metall.* 30 (1982) 1.
13. K. OSAMURA, R. SUZUKI and Y. MURAKAMI, Proceedings of the 4th International Conference on Rapidly Quenched Metals (Japan Institute of Metals, Sendai, 1982) p. 431.
14. H. S. CHEN and C. C. LO, "Rapidly Solidified Metals" (MIT Press, Cambridge, 1976) p. 413.
15. P. I. KRIPYAKEVICH, V. S. PROTASOV and E. E. CHERKASHIN, *Russ. J. Inorg. Chem.* 10 (1965) 151.
16. E. T. HAYES, A. H. ROBERSON and W. L. O'BRIEN, *Trans. ASM* 43 (1951) 888.
17. K. OSAMURA, K. SHIBUE, H. SHINGU and Y. MURAKAMI, *J. Mater. Sci.* 14 (1979) 945.
18. M. F. ASHBY, "Strengthening Methods in Crystals", edited by A. Kelly and R. B. Nicholson (Elsevier Pub. Co. Ltd., Amsterdam, 1971) p. 137.

Received 9 June
and accepted 21 September 1983